Protein Corona Influences Cell–Biomaterial Interactions in Nanostructured Tissue Engineering Scaffolds

Vahid Serpooshan, Morteza Mahmoudi, Mingming Zhao, Ke Wei, Senthilkumar Sivanesan, Khatereh Motamedchaboki, Andrey V. Malkovskiy, Andrew B. Goldstone, Jeffrey E. Cohen, Phillip C. Yang, Jayakumar Rajadas, Daniel Bernstein, Y. Joseph Woo, and Pilar Ruiz-Lozano**

Biomaterials are extensively used to restore damaged tissues, in the forms of implants (e.g., tissue engineered scaffolds) or biomedical devices (e.g., pacemakers). Once in contact with the physiological environment, nanostructured biomaterials undergo modifications as a result of endogenous proteins binding to their surface. The formation of this macromolecular coating complex, known as "protein corona," onto the surface of nanoparticles and its effect on cell–particle interactions are currently under intense investigation. In striking contrast, protein corona constructs within nanostructured porous tissue engineering scaffolds remain poorly characterized. As organismal systems are highly dynamic, it is conceivable that the formation of distinct protein corona on implanted scaffolds might itself modulate cell–extracellular matrix interactions. Here, it is reported that corona complexes formed onto the fibrils of engineered collagen scaffolds display specific, distinct, and reproducible compositions that are a signature of the tissue microenvironment as well as being indicative of the subject's health condition. Protein corona formed on collagen matrices modulated cellular secretome in a context-specific manner ex vivo, demonstrating their role in regulating scaffold–cellular interactions. Together, these findings underscore the importance of custom-designing personalized nanostructured biomaterials, according to the biological milieu and disease state. The use of protein corona as in situ biosensor of temporal and local biomarkers is proposed.

1. Introduction

The surface of nanostructured biomaterials (e.g., nano particles, tubes, and capsules) is covered by various types of macromolecules (e.g., proteins), upon their entrance to the biological fluids.[1–3] The absorption of these biomolecules onto biomaterial surfaces might confer them a new "biological identity."[1,4–6] Therefore, in reality what the cells "see" when interacting with implanted constructs is the protein coated nanostructures (so called "protein corona") on their surface, rather than the pristine materials.[3,7] These protein constructs consist of hard corona (the irreversibly bounded proteins) and soft corona (a dynamic exchange of proteins between the biomaterial surface and media).[8] Accordingly, once administered in vivo, the biological fate of biomaterials could be defined by the type and amount of the associated proteins in the composition of the protein corona.[2,9] For instance, negatively charged, poly(acrylic acid)-conjugated, gold nanoparticles can bind to fibrinogen and change its

Dr. V. Serpooshan, Dr. M. Mahmoudi, Prof. P. C. Yang, Dr. J. Rajadas, Prof. D. Bernstein, Prof. P. Ruiz-Lozano
Stanford Cardiovascular Institute
Stanford, CA 94305, USA
E-mail: mahmoudi@stanford.edu; prlozano@stanford.edu
Dr. V. Serpooshan, Dr. M. Zhao, Prof. D. Bernstein, Prof. P. Ruiz-Lozano
Department of Pediatrics
Stanford University
300 Pasteur Dr., Stanford, CA 94305, USA
Dr. M. Mahmoudi, Prof. P. C. Yang
Division of Cardiovascular Medicine
Stanford University
300 Pasteur Dr., Stanford, CA 94305, USA
Dr. K. Wei
Sanford-Burnham Medical Research Institute
10901 N. Torrey Pines Road, La Jolla, CA 92037, USA
Dr. S. Sivanesan, Dr. A. V. Malkovskiy, Dr. J. Rajadas
Biomaterials and Advanced Drug Delivery Laboratory
Stanford University
300 Pasteur Dr., Stanford, CA 94305, USA
Dr. K. Motamedchaboki
Proteomics Facility
Sanford-Burnham Medical Research Institute
La Jolla, CA 92037, USA
Dr. A. B. Goldstone, Dr. J. E. Cohen, Prof. Y. J. Woo
Department of Cardiothoracic Surgery
Stanford University Medical Center
Stanford, CA 94305, USA

DOI: 10.1002/adfm.201500875

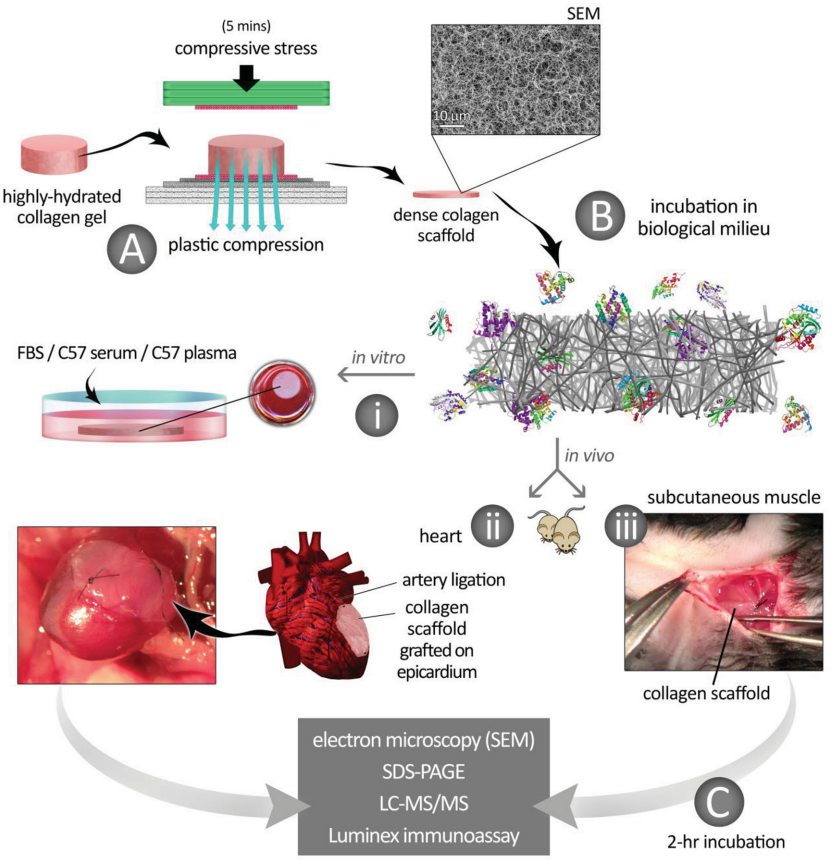

Figure 1. Schematic illustration of the patch-corona study. A) Plastic compression of highly hydrated collagen gels was used to generate a dense fibrillar scaffold structure (i.e., collagen patch).[38,44] The panel on the right shows scanning electron microscopy of the collagen patch fibrillar ultrastructure. B) Collagen scaffolds were incubated in different biological environments including (i) fetal bovine serum, and C57 mouse serum and plasma, in vitro, (ii) onto the sham (healthy) or myocardial infarcted (MI) heart tissue in C57 mouse, in vivo, and (iii) onto the subcutaneous muscle tissue in healthy or MI C57 mouse, in vivo. C) 2 h post incubation under each condition (i)–(iii), patches were removed and the protein coronas formed onto the scaffold were analyzed using SEM, SDS-PAGE, LC-MS/MS, and Luminex (human cytokines) immunoassay.

conformation. This new surface can promote interaction of nanoparticles with the integrin receptor and, consequently, release inflammatory cytokines.[9] The composition, conformation, and the quantity of the proteins constituting the corona medium are strongly dependent on factors including physicochemical properties of biomaterials,[10] incubation temperature[11,12] and time,[13] protein source,[4] and protein concentration.[14]

Although the formation of protein corona at the surface of various nano biomaterials has been investigated,[1,10] there is yet no report on the development of such protein constructs onto nanostructured porous scaffolds and their physiological implications in diverse tissue engineering applications. In addition to serving as a mechanical support, an optimal tissue engineering scaffold also provides an "informative" biomimetic environment for the cells to direct them towards the targeted tissue regeneration pathway(s).[15–18] Whereas a significant amount of research has been conducted on the communications between various cells and scaffolding systems,[19–22] little is known about how the numerous macromolecules (proteins) existing in the biologic media may interact with the implanted biomaterial and its potential effects on the scaffold function. Thus, evaluation of protein corona, formed onto the scaffolds in vivo, may offer a greater understanding of the host tissue response to the implanted biomaterials.

In this study we examined the formation of the protein corona and cell interactions with protein corona, using an in vitro-reconstituted, type I collagen gel scaffold both in vitro and in vivo (**Figure 1**). The composition and the structure of the protein corona were probed under various physiologic conditions, including grafting onto the heart and subcutaneous muscle tissues in several murine disease models.

2. Results and Discussion

Upon their entrance to the body, the surface of biomaterials will be covered by a "protein corona" consisting of a wide variety of biomolecules.[1,4,5] The way cells interact with the scaffold biomaterial strongly depends on the patch–biologic media interactions.[23,24] This study examined the formation of the protein corona onto collagen matrices in various protein environments (Figure 1). We tested the hypothesis that adsorption of various macromolecules, secreted/existing in the local biologic microenvironment, onto the patch biomaterial can be used to analyze the cardiac secretome in normal tissue and during injury, such as myocardial infarction.

2.1. Gel Electrophoresis Analysis of the Hard Protein Corona Formed on Collagen Scaffolds In Vitro

Patch incubation in various in vitro protein media (fetal bovine serum (FBS), and C57 mouse serum and plasma) demonstrated significant differences in the composition and band intensities of protein corona adsorbed on the fibrous scaffold under varying conditions (**Figure 2**A–C). Semi-quantitative densitometry was utilized to further assess the relative amounts of proteins classified by molecular weight (20–50, 50–100, and 100–250 kDa) (Figure 2D), demonstrating significant variations in the protein pattern of scaffold hard coronas. The most striking observation was the association of low molecular weight proteins (M_w < 50 kDa) in the corona composition of C57 plasma samples (with protein concentrations of 50% and 100%) (Figure 2D). The coagulation proteins (e.g., fibrinogen-based proteins) can be responsible for the observed difference of protein profiles from plasma and serum sources. These results were in agreement with our previous findings, demonstrating the variation of protein coronas formed on the surface of superparamagnetic iron oxide nanoparticles incubated in plasma versus serum.[4]

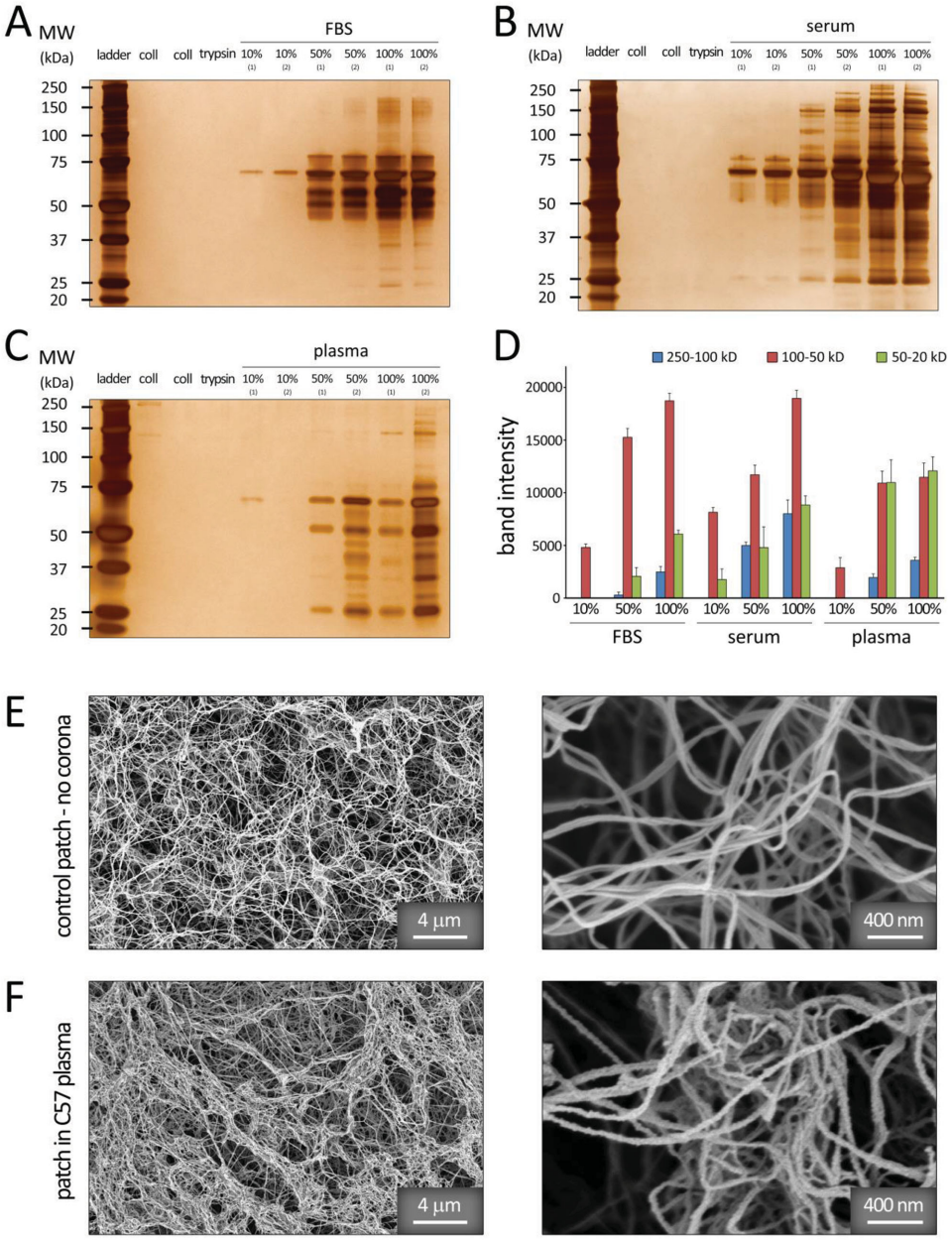

Figure 2. 1D SDS-PAGE hard-corona protein profile for collagen patches incubated with various concentrations of A) FBS, B) C57 mouse serum, and C) C57 mouse plasma proteins. The molecular weights (KDa) of the proteins in the standard ladder are reported on the left for reference. D) Histogram demonstrating the total band intensity of proteins recovered from various corona patches in (A–C). E,F) SEM images of the collagen patch before (E) and after incubation in vitro (in C57 plasma, (F)) confirming the adsorption of various protein macromolecules onto the collagen fibrils.

Incubation in 10% plasma/serum resulted in relatively smaller amount and compositional range of associated proteins in the corona structure, when compared with those formed in 50% and 100% plasma/serum (Figure 2A–D). Higher plasma/serum concentrations yield greater amount of proteins with relatively higher affinity to the biomaterial surface, while the exposed surface remains constant. This results in formation of a thicker, multilayer protein corona at elevated plasma/serum concentrations, which in turn, leads to entrapment of a number of excess proteins within the multilayer structure.[4]

Scanning electron microscopy (SEM) demonstrated the adsorption of various biologic molecules onto the patch and its effect on the fibrillar structure of collagen in vitro (jagged fibrillar surface) (Figure 2E,F).

2.2. Mass Spectrometry—Heatmap Analysis of the Hard Protein Corona Formed on Collagen Scaffolds In Vitro

Liquid chromatography-tandem mass spectrometry (LC-MS/MS) was used to identify the common and unique proteins

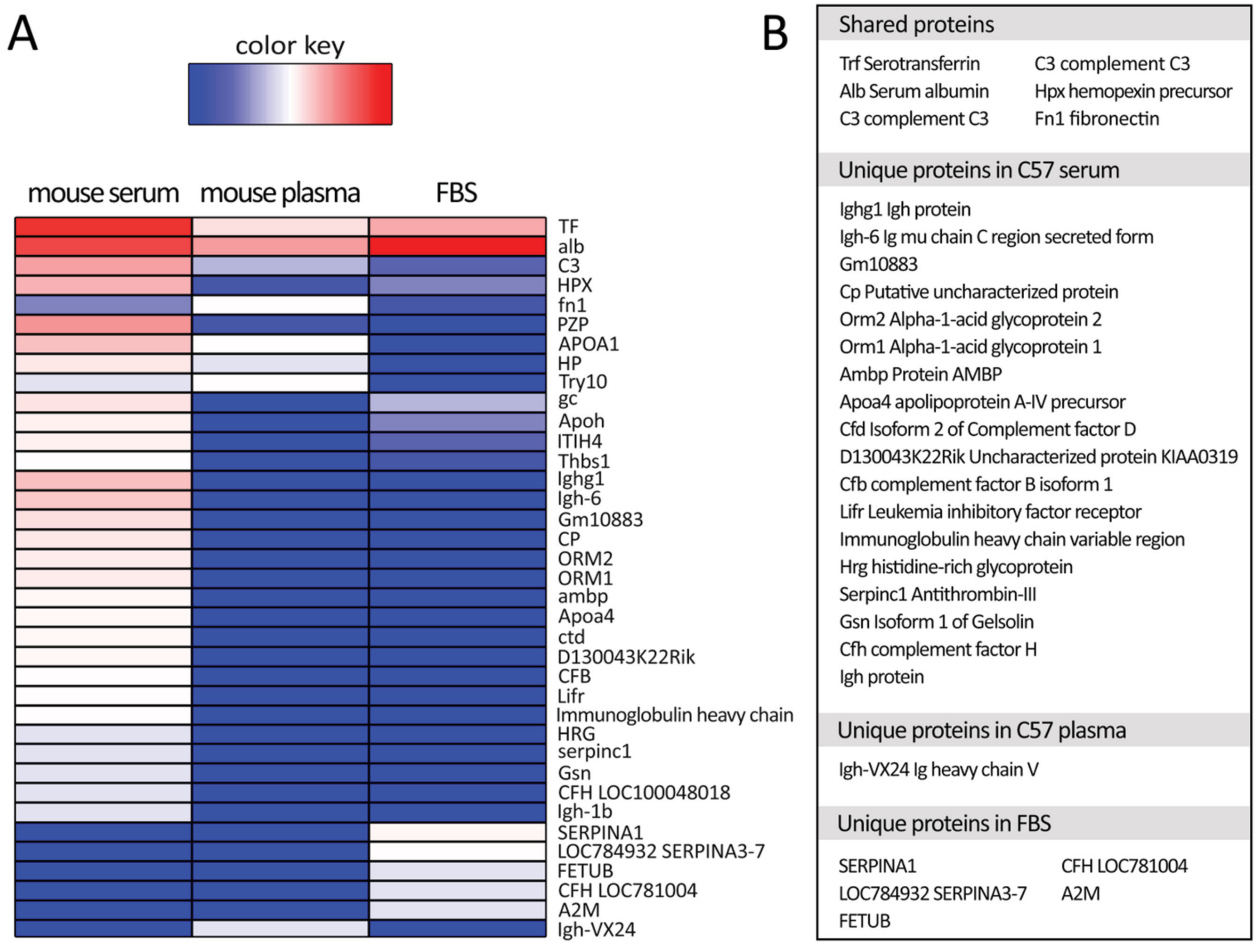

Figure 3. A) Heatmap data visualization of spectral counts of the associated proteins in the corona compositions of various in vitro conditions (C57 mouse serum, C57 muse plasma, and FBS), obtained by mass spectrometry. B) Table lists the proteins shared by C57 serum, plasma and FBS, and proteins unique to each condition.

adsorbed onto the collagen matrices in vitro (**Figure 3**). Their abundances were plotted as a heatmap (Figure 3A) and the shared and unique proteins from each media were identified (Figure 3B). As expected, highly abundant blood proteins were common to all conditions, such as serotransferrin, serum albumin, complement C3, and hemopexin (beta-1B-glycoprotein). However, serum yielded more unique corona proteins (e.g., Ighg1, Orm1 and 2, Ambp, and Apoa proteins) than those found in plasma, suggesting that factors in the plasma prevented the attachment of serum proteins to the scaffold. Greater number of unique proteins in serum versus only one in plasma can be related to the fact that serum is considered as plasma without clotting factors, which suggests that proteins may be able to attach to the scaffold in serum condition more readily than the plasma environment.

2.3. Gel Electrophoresis Analysis of the Hard Protein Corona Formed on Collagen Scaffolds In Vivo

Protein profiles of the collagen patches were also evaluated in vivo, in wild type and severe combined immunodeficient (SCID) mice, and in control (sham) and after myocardial infarction (MI). Patches were inserted in two locations: on the epicardial surface of the heart and in peripheral (subcutaneous) muscle. Sodium dodecyl sulfate polyacrylamide gel electrophoresis (SDS-PAGE) analysis of the extracted patches identified patterns of protein complexes within the fibrillar constructs which were dependent both on the tissue type and physiologic conditions (**Figure 4**). Proteins with mid-range molecular weight (red bars, 50–100 kD) exhibited the greatest band intensities in all conditions. Band intensities declined continuously by subsequent rinses (from PBS1 to 3) (Figure 4B).

2.4. Mass Spectrometry—Heatmap Analysis of the Hard Protein Corona Formed on Collagen Scaffolds In Vivo

Heatmap visualization of spectral counts of proteins detected by LC-MS/MS was generated by hierarchical clustering using total protein spectral count with global normalization (**Figure 5**A). The common serum proteins (serum albumin, serotransferrin, serpin family proteins) and abundant blood cell proteins (hemoglobins)

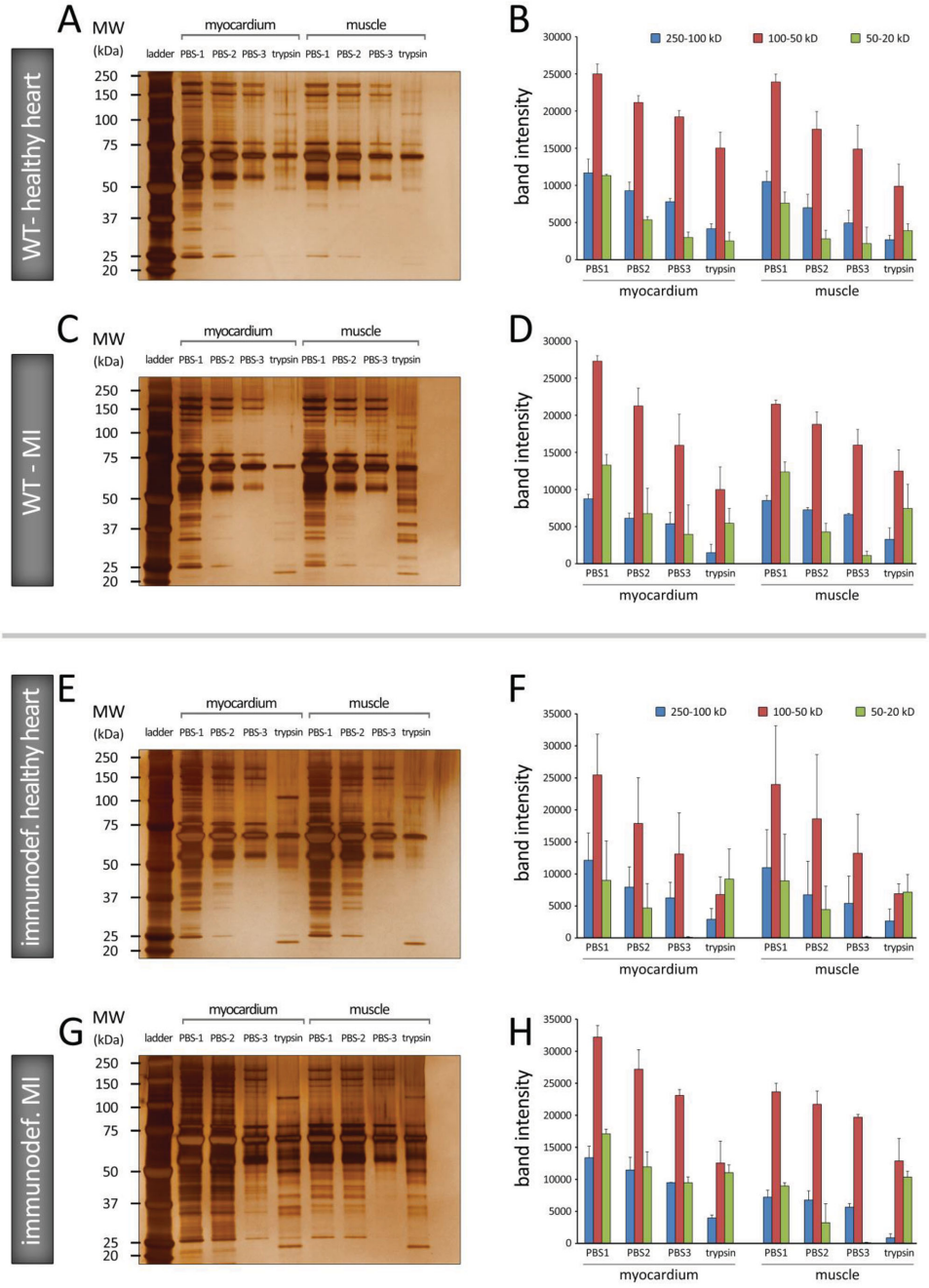

Figure 4. A–D) 1D SDS-PAGE hard-corona protein profile for collagen patches incubated in vivo, in WT C57 BL/6J mice, under healthy heart (A) and (B) and myocardial infarction (MI) conditions (C) and (D) conditions. E–H) 1D SDS-PAGE hard-corona protein profile for patches incubated in immunodeficient C57 (SCID Beige) mice, under healthy heart (E) and (F) and MI (G) and (H) conditions. Each gel image shows the protein corona information of the patches grafted on myocardial (left) and subcutaneous muscle (right) tissues. The molecular weights (KDa) of the proteins in the standard ladder are reported on the left for reference. (B), (D), (F), and (H): Histograms demonstrating the total band intensity of proteins recovered from various corona patches in (A), (C), (E), and (G), respectively.

accounted for the majority of the detected proteins and the overall pattern of detection was similar between the four different conditions. These housekeeping proteins were subsequently subtracted by normalization of the individual protein content in each condition, to highlight the differential detection of proteins (Figure 5B). Individual protein spectral counts are listed in Tables S1–S20, Supporting Information. The majority of the proteins negatively regulated in the SCID condition were components of immunoglobins that are not produced in SCID mice. The absence of immunoglobin-affiliated proteins in the corona structure in the immunodeficient mice suggests that the collagen scaffold representatively captured its surrounding proteins and the corona faithfully recapitulated the in vivo environment that it was embedded into. This may occur due to the significant reduction

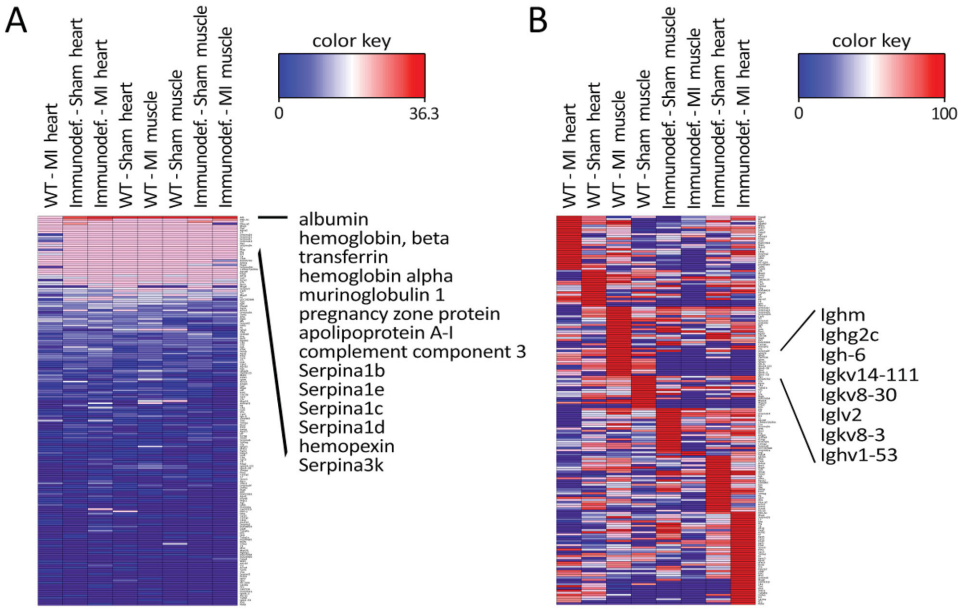

C a

Most changed biological processes (SCID *vs.* Wild type)

Biological Process	P value
acute inflammatory response	2.88E-10
response to wounding	1.35E-09
humoral immune response mediated by circulating immunoglobulin	9.56E-09
humoral immune response	9.06E-08
immunoglobulin mediated immune response	1.99E-07
B cell mediated immunity	2.33E-07
defense response	2.37E-07
inflammatory response	3.56E-07
complement activation, classical pathway	4.41E-07
lymphocyte mediated immunity	5.12E-07

b

Most changed biological processes (MI *vs.* Sham)

Biological Process	P value
response to reactive oxygen species	8.00E-04
oxidation reduction	8.07E-04
cell redox homeostasis	0.002359
cell proliferation	0.002789
response to oxidative stress	0.004588
response to inorganic substance	0.005116
cellular homeostasis	0.006994
cellular response to hydrogen peroxide	0.014045
hydrogen peroxide catabolic process	0.014045
cellular response to reactive oxygen species	0.020997

c

Most changed biological processes (Heart *vs.* subcutaneous muscle)

Biological Process	P value
response to wounding	6.22E-05
response to hydrogen peroxide	0.001099
response to reactive oxygen species	0.00247
cytoskeleton organization	0.004225
muscle system process	0.008335
inflammatory response	0.010817
acute inflammatory response	0.012
response to oxidative stress	0.01375
hyaluronan metabolic process	0.014339
response to inorganic substance	0.015289

Figure 5. Heatmap data visualization of spectral counts of the associated proteins in corona composition obtained from different in vivo conditions: A) showing the total spec count ranking obtained by global normalization; and B) demonstrating expression ranking of normalized individual proteins which associated in corona composition of each in vivo condition. C) Tables listing P values of top 10 significantly changed biological processes between (a) SCID versus wild type, (b) MI versus sham, and (c) heart versus subcutaneous muscle, ranked by P value.

in the concentration of the immunoglobin proteins in the immunodeficient mouse and their consequent affinity changes (reduction) to the surface of nanostructured scaffold.[25,26]

Grouping the protein counts by WT versus SCID, heart versus subcutaneous muscle, and MI versus sham, produced a comparison of altered proteins in the designated groups (Table S1,

Supporting Information) and the top altered biological processes generated through gene ontology (Figure 5C). Most highly changed biological processes in SCID versus WT are related to the immune system, including all immunoglobin proteins, validating that the corona from the scaffold faithfully represented its interacting biologic environment. In the case of MI versus sham our analysis demonstrated the involvement of reactive oxygen species and oxidative stress to be a main biological change during the first 2 h after ischemic injury. In particular, Prdx family genes (Prdx1, 2, 6) were specifically enriched in the MI corona, suggesting the notable presence of these novel peroxidase enzymes in the infarct area. Cytoskeleton organization and muscle system process were among the top changes between heart and subcutaneous muscle, suggesting that tissue specific cells were also attracted to the scaffolds and hence, various intracellular proteins (e.g., Actn2, Actn4, and Tuba4a in Table S1, Supporting Information) abundantly existed in the corona (Figure 5C).

To probe the biosensing capability of the collagen patches, the most enriched proteins binding to scaffolds from in vivo data were defined (Figure S1, Supporting Information). Based on KEGG pathway analysis of significant proteins binding to collagen, we found that the complement and coagulation cascades were the most enriched pathways involved in binding to the collagen patch.

2.5. Assessment of Cell-Biomaterial Interactions in the Presence of Protein Corona

To assess how cells will react to the different protein coronas formed on the collagen patches, human umbilical vein endothelial cells (HUVECs) were cultured onto the matrices extracted after 2 h in vivo implantation (**Figure 6**). Cells showed a normal (healthy) morphology when attached to the fibrillar corona-coated matrices (scanning electron microscopy, Figure 6A). The number of HUVECs attaching to the sham–collagen substrate was qualitatively greater than those attached to MI matrices. Cells cultured on MI versus healthy sham patches showed changes in morphology, with a relative increase in cell surface roughness (jagged cell membrane).

To determine the effect of protein corona-coated matrices on cell metabolism, AlamarBlue reduction was determined following 24 h of culture (Figure 6B). In comparison to the 2D control culture and sham-incubated patches, HUVECs cultured on either 3D patches without corona or MI – incubated patches exhibited significantly reduced metabolic activity ($P < 0.05$).

We further analyzed the pattern of cytokine production (Luminex Immunoassay) of the HUVEC cells after incubation for 24 h with control patch (with no protein corona) and different corona coated-patches (incubated in sham heart, sham muscle, MI heart, and MI muscle) (Figure 6C and Figure S2, Supporting Information). Considerable substrate-dependent differences were observed in the release of positively detected cytokines, including those related to the inflammatory response (e.g., Interleukin-6 (IL6), IL8, monocyte chemotactic protein 1 (MCP1), and tumor necrosis factor beta (TNFB)), cell adhesion properties (e.g., vascular cell adhesion protein 1 (VCAM1)), and fibrinolysis (e.g., plasminogen activator inhibitor-1 (PAI1)). HUVECs cultured on the patches extracted from MI heart released greater levels of IL22, IL23, and IL6, in comparison with those from sham heart (Figure 6C, panel a). In contrast to the heart tissue, sham muscle induced greater levels of cytokine release in comparison to MI muscle (Figure 6C, panel b).

Among the pool of proteins in the plasma, it is well recognized that unfolded fibrinogen has a crucial role in activation of the integrin receptor (Mac-1 pathway), through its C-terminus of the γ chain.[7] Our LC-MS/MS results confirmed that there are significant variations in fibrinogen concentration in the corona compositions of different patches (Tables S1–S20 and Figure S2, Supporting Information). Therefore, one can expect that the observed changes in the inflammatory cytokines could be occurring due to the different decoration of fibrinogen in the corona composition of the patches.

The monocyte chemotactic protein 1 (MCP1) is another inflammatory cytokine that recruits immune cells (e.g., monocytes, T cells, and dendritic cells) into injured tissue.[27] Interestingly, the secretion of MCP1 from HUVEC cells after interaction with various corona coated-patches was significantly higher than the control patch, indicating the effective and accurate role of the corona coated-patch in reflecting the injured tissue microenvironment. In addition, patches obtained from MI heart tissue (with a great level of tissue damage) had the greatest amount of MCP1 compared to the other tissues. It has been shown that the amount of PAI1 cytokine, an inhibitor of fibrinolysis (the process that degrades blood clots[28], is significantly increased after MI.[29] Accordingly, the greatest amount of secreted PAI1 we observed was in the supernatant of HUVEC cells interacted with MI heart tissue patch corona.

The cardiac secretome has recently generated substantial interest as new high-throughput methods for detecting small changes in secreted proteins have been developed.[30–33] The secretome can be utilized to detect new signaling pathways associated with cardiac pathology and therefore new drug targets, as well as to search for novel biomarkers,[34,35] which could then potentially be detected in the plasma. However, current techniques used in animal models such as pericardial fluid analysis[36] or plasma sampling have significant limitations. Our results demonstrate the use of a nanostructured collagen-based scaffold as an in situ biosensor in the studies of various disease biomarker discovery, to directly detect – and collect – the diverse macromolecules that are present (even transiently) in the tissue microenvironment. In terms of its potential clinical application, catheter-based techniques can be used to deliver and apply the biosensor patch system to the target tissue/organ.

3. Conclusion

In summary, we demonstrated the formation of complex protein shells onto fibrillar tissue engineering constructs when they were introduced into various biological environments. The protein corona composition was shown to be a function of tissue type and health condition. Moreover, the interaction between corona-coated collagen matrices with endothelial cells demonstrated a significant effect on cell morphology, viability, and metabolism, as well as the cytokine profile released by cells. Evaluating the potential of such fibrillar scaffold systems

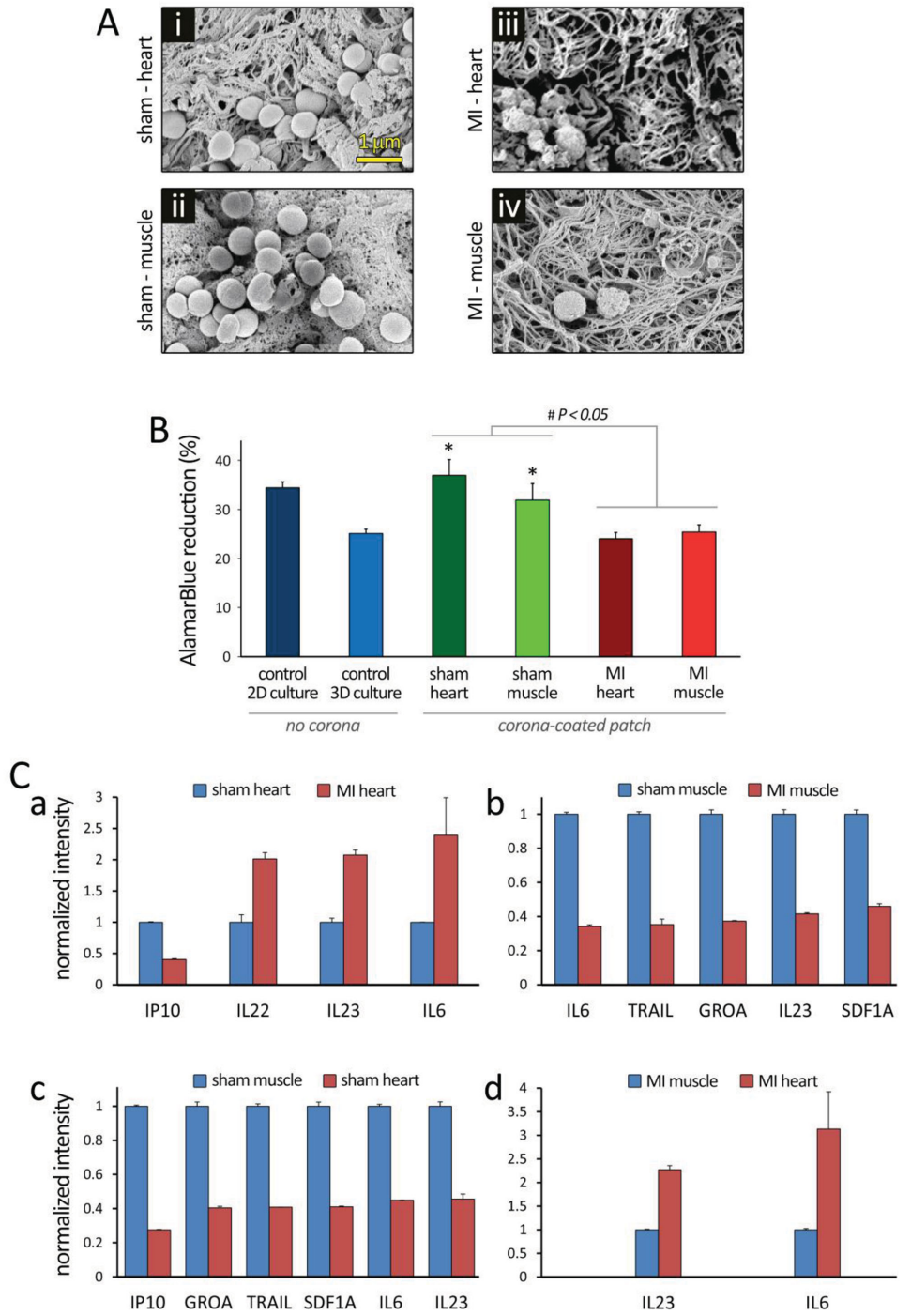

Figure 6. Evaluation of cells interaction with protein corona-patch following 24 h of culture in vitro. Human umbilical vein endothelial cells (HUVECs) were plated onto collagen patches that were previously incubated in different in vivo conditions for 2 h. HUVECs were also cultured on 2D substrate, and on 3D collagen patches, without protein corona, as controls. A) SEM images show HUVECs seeded onto the collagen patches incubated in (i) Sham-heart, (ii) Sham-muscle, (iii) MI-heart, and (iv) MI-muscle tissues. Remarkable differences were observed in the patch fibrillar ultrastructure, protein corona formation, and cell number/attachment. B) AlamarBlue assay demonstrated significantly different HUVEC viability/metabolism under varying conditions ($P < 0.05$). *: Significantly different compared to the 3D culture control ($P < 0.05$). The differences in the means (± SEM) were tested using ANOVA to check for statistical significance ($P < 0.05$). C) The 63-plex Luminex Immunoassay of human cytokines detected significant differences in the production of multiple cytokines in the supernatant of HUVECs, after 24 h of culture in vitro. Patch without cells was used to establish background signal in the assay; values smaller or not significantly greater than background were considered as negative. In all positively detected cytokines, those with levels significantly changed more than two folds between conditions are summarized in panels (a–d).

to serve as a local biosensor/collector would further enable the study of the expression of various emerging biomarkers for different diseases, at the cellular and tissue levels.

4. Experimental Section

Preparation of Collagen Patch: Hydrated collagen gels were fabricated by adding 1.1 mL of 1× Dulbecco's modified eagle medium (DMEM, Sigma, MO, US) to 0.9 mL of sterile, rat tail-derived, type I collagen solution (in acetic acid, 3.84 mg mL^{-1}, Millipore, MA, US) and neutralizing by 0.1 N NaOH in a drop-wise manner.[16,37–39] For the entire patch preparation process, collagen solution was kept on the ice (4 °C) to prevent premature polymerization of the collagen.[40] The collagen solution (0.9 mL) was subsequently cast into the wells of 24-well plates (d = 15.6) and placed in a tissue culture incubator for 30 min at 37 °C for polymerization. Thereupon, highly hydrated collagen gels with poor mechanical integrity were produced.[41–43] To improve the hydrogels physical stability, hydrated collagen gels underwent plastic compression (as previously described[37,41,43]). Briefly, cast collagen gels were removed from the well (used as mold) and transferred to a porous substrate comprising (bottom to top) paper layers, a steel mesh, two polymer meshes, and two fabric meshes (Figure 1A). By applying a static compressive stress of 1400 N m^{-2} to the scaffold, for 5 min, the excess fluid was expelled out of the construct, yielding a dense biomaterial (Figure 1B) with improved biomechanical properties.[16,38,44] Compressed collagen sheets (used as collagen patch) were then transferred to and rinsed in PBS (using the fabric mesh) before incubating in various media.

Extraction of Protein Corona In Vitro: Collagen patches were incubated at different concentrations (10%, 50%, and 100%) of various protein sources including FBS, C57-serum, and C57-plasma. Scaffolds were immersed in 1 mL of protein solution (in 24 well plates) and incubated for 2 h in the tissue culture incubator (37 °C – 5% CO_2). Following the incubation in protein source, the supernatants were completely removed and the patches were extensively washed with PBS (three times, 5 min each, on the shaker), in order to dislodge loosely attached proteins (aka, "soft corona") from the 3D structure of the patch. Subsequently, to remove the more strongly attached proteins (aka, "hard corona") from the collagen constructs, patches were immersed in 1 mL of trypsin (0.05%, HyClone 1X, SH40003.12) for 5 min and the supernatants were collected. The obtained solutions were used for gel electrophoresis and mass spectroscopy analysis.

Mouse Model of Myocardial Infarction—Patch Implantation: All procedures involving animal use, housing, and surgeries were approved by the Stanford Institutional Animal Care and Use Committee (IACUC). Animal care and interventions were provided in accordance with the Laboratory Animal Welfare Act. Male, 10–13 weeks old, wild type (C57BL/6J), and SCID Beige mice were purchased from Jackson Laboratories (Bar Harbor, ME, USA) and studied in four different groups: (I) healthy myocardium, (II) myocardial infarction (MI), (III) immunodeficient mouse with healthy myocardium, and (IV) immunodeficient mouse with MI. In each group, the patch was grafted onto both the epicardium and the extra-thoracic subcutaneous muscle (Figure 1B, n = 4 per group). Mice were anesthetized utilizing an isoflurane inhalational chamber (2%). This was followed by endotracheal intubation using a 20-gauge angiocatheter (Becton, Dickinson Inc., Sandy, Utah) that was connected to a small animal volume-control ventilator (Harvard Apparatus, Holliston, MA). A left thoracotomy was performed via the fourth intercostal space and the lungs retracted to expose the heart. For the mice with MI, once the pericardium was opened, a 7–0 suture was placed to ligate the left anterior descending artery (LAD) approximately 2 mm below the left atrial appendage. Criterion for occlusion success was an immediate color change in the left ventricular (LV) anterolateral wall (red turning to pale gray). In each animal group, two prepared collagen patches were implanted: 1 – one patch was sutured (at two points) onto the ischemic/healthy myocardium, and 2 – another patch was placed onto the subcutaneous muscle (no suture), after closing the intercostal space (Figure 1B). The incision was then closed and animals were kept on a heating pad until they were extubated and recovered.

Extraction of Protein Corona In Vivo: 2 h after patch implantation into the various mice groups, the animals were scarified and the patches were extracted from heart and muscle tissues. The extracted collagen scaffolds were then briefly rinsed with saline (20 s) to remove the blood and nonattached residues. To obtain the in vivo profile of (soft) protein corona complexes formed on the patches, patches were extensively rinsed with PBS (three times, 5 min each, on the shaker), and supernatant solutions were collected for further analysis. The patches were then immersed in 1 mL of trypsin (0.05%) for 5 min for removing the attached proteins with higher affinities (hard corona).

Sodium Dodecyl Sulfate Poly-acrylamide Gel Electrophoresis (SDS-PAGE): Supernatant solutions obtained from various rinsing steps described above were separately mixed with loading buffer [62.5×10^{-3} M Tris-HCL pH 6.8, 2% (w/v) SDS, 10% glycerol, 0.04 M dithiothreitol (DTT), and 0.01% (w/v) bromophenol blue], followed by boiling for 5 min at 100 °C. An equal sample volume was loaded in 12% gel polyacrylamide gel. Gel electrophoresis was performed at 120 V, 400 mA for ≈60 min each, until the proteins neared the end of the gel. The gels were stained with silver staining kit. Gels were then scanned using a calibrated densitometer scanner (Bio-Rad Molecular Imager Gel Doc XR+ Imaging System) and gel densitometry was performed using image J (1.410).

Liquid Chromatography-Tandem Mass Spectrometry (LC-MS/MS): Proteins adsorbed on the collagen scaffolds were digested using filter-aided sample preparation (FASP) method.[45] Proteins reduction and alkylation were carried in presence of 8 M urea on filter by adding DTT (10×10^{-3} M final concentration) and incubating at 32 °C for 60 min using thermomixer set on 800 rpm. Iodoacetamide was added (to 30×10^{-3} M final concentration) and proteins were alkylated for 20 min at room temperature, in the dark and on thermomixer set at 800 rpm. Mass spectrometry grade trypsin (Promega) was added (1:50 ratio) for overnight digestion at 32 °C on thermomixer. After digestion and peptide elution, formic acid was added to the peptide solution (to 1%), followed by drying the sample to 150 µL and desalting by peptide microtrap (Michrom-Bruker, TR1/25109/02). Desalted peptides were resuspended in 50 µL of 5% ACN in 0.1% formic acid/water; followed by on-line analysis of 20% of total digests by high-resolution, high-accuracy LC-MS/MS, consisting of a Michrom 1D HPLC, a 15 cm Michrom Magic C18 column, a captive spray Michrom source, and LTQ-Orbitrap Velos Pro with ETD (Thermo Fisher Scientific). A 45 min gradient of 10%–30% B (0.1% formic acid, 100% acetonitrile) was used to separate the peptides. The LTQ-OrbiTrap Velos Pro was set to scan precursors in the OrbiTrap followed by data-dependent MS/MS of the top 10 precursors and a column heater set to 27 °C during the LC-MS/MS runs. Sorcerer Enterprise v.3.5 release (Sage-N Research Inc.) with SEQUEST algorithm was used as the search program for peptide/protein identification. SEQUEST parameters were set to search the target-decoy ipi.MOUSE.vs3.73 and ipi.BOVINE.vs3.72 fasta protein database; containing protein sequences using trypsin for enzyme with the allowance of up to 2 missed cleavages, semi tryptic search and precursor mass tolerance of 50 ppm. Differential search included methionine oxidation (16 Da) and cysteines carboxyamidomethylation (57 Da). The search results were viewed, sorted, filtered, and statically analyzed by comprehensive proteomics data analysis software, peptide/protein prophet v.4.02 (ISB). In this study, the trans-proteomic pipeline (TPP) protein minimum probability was set to 0.95, to assure very low error (much less than FDR 1%) with reasonably good sensitivity. The differential spectral count analysis was done by QTools, an automated differential peptide/protein spectral count and Gene Ontology analysis tool.[46] To determine the total number of the mass spectra for the all peptides attributed to a matched protein, a semi-quantitative assessment of the protein amount was conducted through application of the spectral counting (SpC) method by applying the following equation

$$NpSpC_k = \left(\frac{SpC / (M_w)_k}{\sum_{i=1}^{n} (SpC/(M_w)_i)} \right) \times 100 \quad (1)$$

where $NpSpC_k$ is the normalised percentage of the spectral count for protein k, SpC is the spectral count identified, and M_w is the molecular weight (in kDa) of protein k.

Scanning Electron Microscopy (SEM) of Patch-Corona: To investigate the ultrastructural changes in the collagen scaffolds as a result of interaction with the biologic milieu, patches pre and postincubation with biologic media were analyzed using scanning electron microscopy (Zeiss Sigma field emission microscope, FESEM, Carl Zeiss Microscopy, NY) operated at 1–2 kV, using InLens SE detection. Collagen scaffolds were fixed by immersion in 4% paraformaldehyde solution overnight and washed twice with 0.1 M sodium cacodylate buffer (pH 7.4) and then post-fixed in 1% aqueous osmium tetroxide (OsO_4) for 1 h. Samples were then washed twice in purified water and dehydrated in an increasing ethanol solution series (50, 70, 90, and 100%, 2 × 15 min each). Finally, the specimens were critical-point dried (CPD) in liquid CO_2, in a Tousimis 815B critical-point dryer (Tousimis, MD). CPD-dried samples were mounted on standard SEM stubs with adhesive copper tape and sputter-coated with 4 nm of Au/Pd in a Denton Desk II machine (Denton Vacuum, NJ).

Cell Culture and Metabolic Activity Assay: HUVECs were plated (at a density of 100 000 cells mL^{-1}) onto the collagen matrices obtained following 2 h incubation with different biologic media and were cultured in CS-C medium (Sigma, MO, US) supplemented with 10% fetal bovine serum (FBS, Sigma) in a humidified incubator at 37 °C using 5% CO_2. AlamarBlue (Invitrogen Inc., Carlsbad, CA) was used to measure the metabolic activity of HUVECs as an indicator of cell viability and growth. Following 24 h of culture, the medium was renewed and AlamarBlue reagent was added to each well at 10% of the culture volume. Samples were then incubated at 37 °C for 4 h. Acellular scaffolds were used for background reference subtraction. The absorbance of 100 µL of medium was read at 550 and 595 nm using a microplate reader (Cytation 3 Cell Imaging Multi-Mode Reader, BioTek Instruments, Inc., VT, US) and the percentage of reduced AlamarBlue was calculated according to the manufacturer's instructions.

Luminex—eBiosciences/Affymetrix Magnetic Bead Kit: This assay was performed in the Human Immune Monitoring Center at Stanford University. Patch without cells was used as background signal. Values smaller than background were considered as negative and omitted. Moreover, mouse cytokines that were cross-reactive with human panel were disregarded. Median florescence intensities of 63 human cytokines were probed in the supernatant culture media of the HUVEC cells after incubation for 24 h. Human 63-plex kits were purchased from eBiosciences/Affymetrix and used according to the manufacturer's recommendations with modifications as described below. Briefly, beads were added to a 96-well plate and washed in a Biotek ELx405 washer. Samples were added to the plate containing the mixed antibody-linked beads and incubated at room temperature for 1 h followed by overnight incubation at 4 °C with shaking. Cold and room temperature incubation were performed on an orbital shaker at 500–600 rpm. Following the overnight incubation, plates were washed in a Biotek ELx405 washer and then biotinylated detection antibody added for 75 min at room temperature with shaking. Plate was washed and streptavidin-PE was added. Following incubation for 30 min at room temperature, wash was performed as above and reading buffer was added to the wells. Each sample was measured in duplicate. Plates were read using a Luminex 200 instrument with a lower bound of 50 beads per sample per cytokine. Custom assay control beads by Radix Biosolutions were added to all wells.

Statistical Analysis: The number of samples (n) used in each experiment is noted in the text. Dependent variables are expressed as means ± SEM. The differences in the means were tested using ANOVA and Student T-test to check for statistical significance ($P < 0.05$).

Supporting Information

Supporting Information is available from the Wiley Online Library or from the author.

Acknowledgements

V.S. and M.M. contributed equally to this work. This work was supported by National Institutes of Health grants HL65484 and HL086879 (to P.R.-L.) and NIH R01 HL095571 (to Y.J.W.). V.S. was an Oak Foundation postdoctoral fellow at Stanford. D.B. was supported by NIG grant HL061535. K.W. was a SBMRI California Institute for Regenerative Medicine postdoctoral fellow (TG2-01162).

Received: March 4, 2015
Revised: May 5, 2015
Published online: June 5, 2015

[1] M. P. Monopoli, C. Åberg, A. Salvati, K. A. Dawson, *Nat. Nanotechnol.* **2012**, *7*, 779.
[2] M. P. Monopoli, F. B. Bombelli, K. A. Dawson, *Nat. Nanotechnol.* **2011**, *6*, 11.
[3] I. Lynch, A. Salvati, K. A. Dawson, *Nat. Nanotechnol.* **2009**, *4*, 546.
[4] S. Laurent, C. Burtea, C. Thirifays, F. Rezaee, M. Mahmoudi, *J. Colloid Interface Sci.* **2013**, *392*, 431.
[5] M. Mahmoudi, S. N. Saeedi-Eslami, M. A. Shokrgozar, K. Azadmanesh, M. Hassanlou, H. R. Kalhor, C. Burtea, B. Rothen-Rutishauser, S. Laurent, S. Sheibani, H. Vali, *Nanoscale* **2012**, *4*, 5461.
[6] P. M. Kelly, C. Åberg, E. Polo, A. O'Connell, J. Cookman, J. Fallon, Ž. Krpetić, K. A. Dawson, *Nat. Nanotechnol.* **2015**, *10*, 472.
[7] D. Walczyk, F. B. Bombelli, M. P. Monopoli, I. Lynch, K. A. Dawson, *J. Am. Chem. Soc.* **2010**, *132*, 5761.
[8] M. Mahmoudi, M. A. Shokrgozar, S. Sardari, M. K. Moghadam, H. Vali, S. Laurent, P. Stroeve, *Nanoscale* **2011**, *3*, 1127.
[9] Z. J. Deng, M. Liang, M. Monteiro, I. Toth, R. F. Minchin, *Nat. Nanotechnol.* **2011**, *6*, 39.
[10] M. Mahmoudi, I. Lynch, M. R. Ejtehadi, M. P. Monopoli, F. B. Bombelli, S. Laurent, *Chem. Rev.* **2011**, *111*, 5610.
[11] M. Mahmoudi, A. M. Abdelmonem, S. Behzadi, J. H. Clement, S. Dutz, M. R. Ejtehadi, R. Hartmann, K. Kantner, U. Linne, P. Maffre, S. Metzler, M. Moghadam, C. Pfeiffer, M. Rezaie, P. Ruiz-Lozano, V. Serpooshan, M. Shokrgozar, G. U. Nienhaus, W. J. Parak, *ACS Nano* **2013**, *7*, 8379.
[12] M. Mahmoudi, S. E. Lohse, C. J. Murphy, A. Fathizadeh, A. Montazeri, K. S. Suslick, *Nano Lett.* **2014**, *14*, 6.
[13] S. Tenzer, D. Docter, J. Kuharev, A. Musyanovych, V. Fetz, R. Hecht, F. Schlenk, D. Fischer, K. Kiouptsi, C. Reinhardt, K. Landfester, H. Schild, M. Maskos, S. K. Knauer, R. H. Stauber, *Nat. Nanotechnol.* **2013**, *8*, 772.
[14] M. P. Monopoli, D. Walczyk, A. Campbell, G. Elia, I. Lynch, F. B. Bombelli, K. A. Dawson, *J. Am. Chem. Soc.* **2011**, *133*, 2525.
[15] M. Mahmoudi, S. Bonakdar, M. A. Shokrgozar, H. Aghaverdi, R. Hartmann, A. Pick, G. Witte, W. J. Parak, *ACS Nano* **2013**, *7*, 8379.
[16] V. Serpooshan, M. Julien, O. Nguyen, H. Wang, A. Li, N. Muja, J. E. Henderson, S. N. Nazhat, *Acta Biomater.* **2010**, *6*, 3978.
[17] R. G. Breuls, T. U. Jiya, T. H. Smit, *Open Orthop. J.* **2008**, *2*, 103.
[18] D. E. Discher, P. Janmey, Y. L. Wang, *Science* **2005**, *310*, 1139.
[19] C. M. Murphy, F. J. O'Brien, D. G. Little, A. Schindeler, *Eur. Cell. Mater.* **2013**, *26*, 120.
[20] J. Venugopal, S. Low, A. T. Choon, S. Ramakrishna, *J. Biomed. Mater. Res. B Appl. Biomater.* **2008**, *84*, 34.
[21] M. Spector, *Tissue Eng.* **2002**, *8*, 351.

[22] H. Chen, Y. Liu, Z. Jiang, W. Chen, Y. Yu, Q. Hu, *Exp. Cell Res.* **2014**, *323*, 346.
[23] M. P. Monopoli, C. Åberg, A. Salvati, K. A. Dawson, *Nat. Nanotechnol.* **2012**, *7*, 779.
[24] D. Walczyk, F. B. Bombelli, M. P. Monopoli, I. Lynch, K. A. Dawson, *J. Am. Chem. Soc.* **2010**, *132*, 5761.
[25] M. Ghavami, S. Saffar, B. A. Emamy, A. Peirovi, M. A. Shokrgozar, V. Serpooshan, M. Mahmoudi, *RSC Adv.* **2012**, *3*, 1119.
[26] M. P. Monopoli, D. Walczyk, A. Campbell, G. Elia, I. Lynch, F. Baldelli Bombelli, K. A. Dawson, *J. Am. Chem. Soc.* **2011**, *133*, 2525.
[27] M. W. Carr, S. J. Roth, E. Luther, S. S. Rose, T. A. Springer, *Proc. Natl. Acad. Sci. U.S.A.* **1994**, *91*, 3652.
[28] B. R. Binder, G. Christ, F. Gruber, N. Grubic, P. Hufnagl, M. Krebs, J. Mihaly, G. W. Prager, *News Physiol. Sci. Int. J. Physiol. Prod. Jointly Int. Union Physiol. Sci. Am. Physiol. Soc.* **2002**, *17*, 56.
[29] A. Panahloo, V. Mohamed-Ali, R. P. Gray, S. E. Humphries, J. S. Yudkin, *Atherosclerosis* **2003**, *168*, 297.
[30] F. de la Cuesta, G. Alvarez-Llamas, F. Gil-Dones, V. M. Darde, E. Calvo, J. A. López, F. Vivanco, M. G. Barderas, *Methods Mol. Biol. Clifton NJ* **2013**, *1005*, 237.
[31] X. Li, Y. Ren, V. Sorokin, K. K. Poh, H. H. Ho, C. N. Lee, D. de Kleijn, S. K. Lim, J. P. Tam, S. K. Sze, *J. Proteomics* **2014**, *98*, 138.
[32] M. Shimano, N. Ouchi, K. Walsh, *Circulation* **2012**, *126*, e327.
[33] F. Vivanco, J. L. Martín-Ventura, M. C. Duran, M. G. Barderas, L. Blanco-Colio, V. M. Dardé, S. Mas, O. Meilhac, J. B. Michel, J. Tuñón, J. Egido, *J. Proteome Res.* **2005**, *4*, 1181.
[34] P. A. Duffy, G. Betton, S. Horner, J. Horner, P. Cotton, N. McMahon, C. Lawrence, H. Prior, D. Armstrong, K. Philp, R. A. Roberts, *Eur. J. Cancer Suppl.* **2007**, *5*, 143.
[35] J.-C. Tardif, T. Heinonen, D. Orloff, P. Libby, *Circulation* **2006**, *113*, 2936.
[36] C. Bang, S. Batkai, S. Dangwal, S. K. Gupta, A. Foinquinos, A. Holzmann, A. Just, J. Remke, K. Zimmer, A. Zeug, E. Ponimaskin, A. Schmiedl, X. Yin, M. Mayr, R. Halder, A. Fischer, S. Engelhardt, Y. Wei, A. Schober, J. Fiedler, T. Thum, *J. Clin. Invest.* **2014**, *124*, 2136.
[37] V. Serpooshan, T. M. Quinn, N. Muja, S. N. Nazhat, *Acta Biomater* **2013**, *9*, 4673.
[38] V. Serpooshan, M. Zhao, S. A. Metzler, K. Wei, P. B. Shah, A. Wang, M. Mahmoudi, A. V. Malkovskiy, J. Rajadas, M. J. Butte, D. Bernstein, P. Ruiz-Lozano, *Biomaterials* **2013**, *34*, 9048.
[39] V. Serpooshan, N. Muja, B. Marelli, S. N. Nazhat, *J. Biomed. Mater. Res. A* **2011**, *96*, 609.
[40] V. V. Artym, K. Matsumoto, *Curr. Protoc. Cell Biol.* **2010**, *10*, 1.
[41] E. A. Abou Neel, U. Cheema, J. C. Knowles, R. A. Brown, S. N. Nazhat, *Soft Matter* **2006**, *2*, 986.
[42] R. A. Brown, M. Wiseman, C. B. Chuo, U. Cheema, S. N. Nazhat, *Adv. Funct. Mater.* **2005**, *15*, 1762.
[43] V. Serpooshan, T. M. Quinn, N. Muja, S. N. Nazhat, *Soft Matter* **2011**, *7*, 2918.
[44] V. Serpooshan, M. Zhao, S. A. Metzler, K. Wei, P. B. Shah, A. Wang, M. Mahmoudi, A. V. Malkovskiy, J. Rajadas, M. J. Butte, D. Bernstein, P. Ruiz-Lozano, *Bioengineered* **2014**, *5*, 193.
[45] J. R. Wiśniewski, A. Zougman, N. Nagaraj, M. Mann, *Nat. Methods* **2009**, *6*, 359.
[46] L. M. Brill, K. Motamedchaboki, S. Wu, D. A. Wolf, *Methods* **2009**, *48*, 311.